THE ASTROPHYSICAL JOURNAL, 308:499–509, 1986 September 15

VELOCITY FIELDS AROUND RICH CLUSTERS OF GALAXIES

JENS V. VILLUMSEN
Institute of Advanced Study; and Department of Astronomy, University of California at Berkeley
AND
MARC DAVIS
Department of Astronomy and Department of Physics, University of California at Berkeley
Received 1985 December 9; accepted 1986 February 27

ABSTRACT

We study the nature of the velocity field around large clusters in $\Omega = 1$ cosmological n-body simulations that have initial conditions which produce large-scale structure reasonably consistent with observations. Our purpose is to test the accuracy of the spherical infall models commonly used to measure the mass of the Virgo supercluster and to characterize the nature of the deviations from simple spherical infall. The measured infall velocity systematically deviates in the mean by less than 20% for shells of mean overdensity $\bar{\delta} < 3$, but only when the infall is averaged over 4π sr. Large asphericities in the flow field are very common, even in the outer regions of the clusters. These asphericities result from the substantial subclustering seen on small scales in all the models, as well as the aspherical nature of the exterior mass distribution. The use of a spherical model for the Virgocentric flow as a measure of Ω is shown to be subject to large systematic and random errors. A much better test is to use a local criterion, noting that local peculiar velocity tracks the direction and amplitude of the local peculiar gravitational force extremely well. This relationship, which must occur in linear theory, can be surprisingly well extended into the nonlinear perturbations of the developing clusters.

Subject headings: cosmology — galaxies: clustering — numerical methods

I. INTRODUCTION

The study of the flowfield around the Virgo Cluster is a unique opportunity to measure the mass of a system on a scale much larger than is possible using virial theorem analyses around more distant clusters. This occurs, of course, because Virgo is sufficiently close for us to measure distances independently of redshift to precision adequate to decide whether a particular galaxy is in front of or behind the cluster center, and by how much. A review of measurements of the flowfield around Virgo has been given by Davis and Peebles (1983). New results include the work of Aaronson *et al.* (1986) and de Vaucouleurs and Peters (1984).

The applications of the large-scale measurement are to test the validity of the assumption that galaxies trace the mass distribution, to determine whether mass-to-light ratios are independent of distance beyond megaparsec scales, and whether estimates of Ω on smaller scales are reliable measures of the true cosmological density. Many models of the formation of structure have suggested that the universe contains substantial material unclustered on small scales, or on any scales (Davis *et al.* 1981; Turner, Steigman, and Kraus 1984; Gelmini, Schramm, and Valle 1984; Olive, Seckel, and Vishniac 1985; Suto, Kodama, and Sato 1985; Efstathiou 1985). Still other recent models suggest that galaxies are "biased" tracers of mass and are more clustered than the underlying matter (Kaiser 1984; Bardeen *et al.* 1985; Davis *et al.* 1985; Peacock and Heavens 1985). These models generally predict that the mass-to-light ratio of gravitating systems should increase with measurement scale. An accurate measurement of mass on the scale of Virgo (15 Mpc) is therefore the best available test of these conjectures.

The test of Virgocentric flow has two aspects. One assumes that galaxies do trace the mass on this large scale and then one computes the observed galaxy overdensity toward Virgo, characterizing it as either a mean overdensity $\bar{\delta}$ within the sphere centered on Virgo with our Virgocentric radius (Silk 1974, 1977; Peebles 1980), or by direct computation of the anisotropy of the gravitational force of all the galaxies in a complete sample (Davis and Huchra 1982). This measure of the gravitational force is then compared to a peculiar velocity v_p, determined by anisotropy measures of the local Hubble flow. In a spherical model, v_p should be the average radial infall velocity or departure from Hubble flow $\bar{V}_r$ at a given radius r and would be determined from some measure of the local shear field. In the spherical model the infall velocity is well approximated both in the linear and nonlinear zones (for $\bar{\delta} < 10$) (Meiksin 1985; Yahil 1985) by

$$\frac{\bar{V}_r}{Hr} \approx \frac{\Omega^{0.6}}{3}\bar{\delta}\left[1+\left(\frac{\bar{\delta}}{3}\right)\right]^{-1/2}. \quad (1)$$

The exact form is given by parametric solution of the Friedmann equation. The difficulty is that Virgo is not spherical but is rather flattened, with our Galaxy located in the plane of flattening, the supergalactic plane. The above formula for a spherical model is therefore only a rough guide. One indication of a possible problem is that the microwave dipole anisotropy, which measures our velocity relative to the comoving frame, has an amplitude of 600 ± 50 km s^{-1}, directed 45° from the Virgo Cluster (Fixsen, Cheng, and Wilkinson 1983; Lubin, Epstein, and Smoot 1983). Perhaps the microwave anisotropy has been largely generated by some more distant mass inhomogeneity, but if it is dominated by Virgo, then the substantial transverse velocity must have been generated by some nonspherical effect. The transverse velocity cannot simply represent a random initial velocity because initial transverse velocities decay adiabatically in an expanding universe. Another discrepancy arises in the component of peculiar velocity directed toward Virgo. The observational studies that focus

on the shear field of galaxies mostly within the local supercluster ($cz < 3000$ km s^{-1}) are best fitted by an infall velocity of 200–300 km s^{-1}, compared to 420 ± 30 km s^{-1} given by the microwave component directed toward Virgo (Davis and Peebles 1983). Some observational studies that measure the shear field at larger distance, beyond the influence of the local supercluster, yield peculiar velocities consistent with the microwave anisotropy (Aaronson *et al.* 1986; Tonry and Davis 1981, but see Dressler 1984). The usual interpretation is that the Local Supercluster is itself moving at 300–450 km s^{-1} in the direction given by the vector difference of the microwave velocity and our infall velocity to Virgo (Tammann and Sandage 1985). The veracity of this conclusion is dependent on the accuracy and absence of systematic biases of the spherical model fit to the local shear field.

Alternative models to address this and other worries have been suggested for Virgocentric flow, such as a homogeneous ellipsoid (White and Silk 1979), a flattened homogeneous pancake (Szalay and Silk 1983), a linear but nonspherical cluster (Davis and Huchra 1982), and allowance for large-scale density fluctuations beyond Virgo (Vittorio and Silk 1985). Each of these models is mathematically tractable, but none is a particularly better approximation to Virgo than the simple spherical model. The Virgo galaxy distribution is quite centrally condensed and is nonlinear, since $\bar{\delta}$ at our radius is 2.0 ± 0.2 (Davis and Huchra 1982). Furthermore, the exterior density field is usually ignored in these models, i.e., assumed to be spherically symmetric, an approximation that again is made for mathematical convenience but which may obviate an accurate mass determination and lead to systematic errors. Testing the validity of these models observationally is extremely difficult.

It is apparent therefore that n-body techniques might lend some guidance to the nature of the expected flow field around Virgo and other clusters. Large cosmological n-body simulations with random phase initial conditions will naturally produce large clusters with substantial substructure and no particular symmetry surrounded by other clusters and voids. Of course all 6 degrees of freedom are known for each particle in a simulation, so it is a simple matter to test the accuracy of the spherical infall model, or of any other model. This paper discusses such comparisons based on a number of n-body simulations run with two different simulation codes, and with several different classes of initial conditions similar to that expected in a universe dominated by cold dark matter. Most of the results to be discussed below are independent of the initial conditions. In short, we do find a number of systematic errors that affect Virgocentric flow analyses based on spherical models, but there is an effective remedy that should be used in future studies. Previous but less detailed comparisons of cluster velocity fields to n-body models have been made by Melott (1983) and by Bushouse *et al.* (1985). They studied models with random Poisson initial conditions and with initial conditions appropriate to a universe dominated by massive neutrinos; our conclusions based on different initial conditions are entirely consistent with theirs.

The plan of this paper is as follows: in § II we discuss the n-body models and the selection of clusters from these models. Section III describes the tests applied to the data, including searches for extensions of the simple spherical model. The mean radial velocity follows the simple spherical model for $\bar{\delta} < 2$ but is systematically low for higher overdensities. We describe expansions of the velocity and force fields in terms of spherical harmonics to the quadrupole order. Substantial dipole and quadrupole distortions in velocity are very common, both in the radial and transverse direction. The asphericity of the interior field is found to be poorly correlated with either the asphericity of the velocity or force fields, indicating the importance of the exterior mass distribution. Section IV describes the comparison of the force field with the velocity field, which in every cluster is excellent. Section V then applies the lessons learned to clusters in the real universe. Section VI is a summary of our conclusions.

II. THE MODELS

We have used for this project models run with a (PM) code written by J. V. V. and with a (PPPM) code of Efstathiou *et al.* (1985). All models were evolved with 32,768 particles using an Einstein–de Sitter $\Omega = 1$ cosmology. The PM code has the capability of higher resolution along one axis and is optimized for study of pancake collapse (Villumsen and Gunn 1985). However, we did not use this feature for this project. We selected 14 clusters from five different simulations of the PM code. The initial conditions were in all cases appropriate to a cold dark matter initial spectrum with random initial phases, which effectively was a power law of slope -1.5 over the dynamic range available in the simulation (Blumenthal and Primack 1983). In three of the runs from which we extracted nine clusters the fundamental wave was amplified along the Z axis above the rms expected value; in two runs the enhancement was a factor of 3; in the other run, the enhancement was a factor of 2. We term these models anisotropic, since the strongest clusters tended to form in the X-Y plane. The remaining runs are all isotropic as there is no preferred orientation of the large-scale structure. Five clusters were selected from two PPPM runs with random phase, power-law initial conditions $|\delta_k|^2 \propto k^n$, $n = -1$ and -2. These runs are taken from a project to study self-similarity behavior in gravitational clustering (Frenck *et al.* 1986).

The effective force softening length in the PM models is $L/64$, where L is the size of the box. In the PPPM models the softening length is less than $L/213$, and these models are therefore much preferred for following details of structures collapsing in comoving coordinates (Efstathiou *et al.* 1985). In the present situation the cluster size is much larger than the force-softening length in either model, and therefore the PM models can be used to address the limited questions of this paper. The PPPM models, with their stronger short-range forces, exhibit larger amplitude small-scale velocity fields, but the large-scale behaviors are virtually indistinguishable, as shown below. Since it is well known that $\Omega \approx 0.1$ if galaxies accurately trace the mass on the scale size of clusters, all of our $\Omega = 1$ models are too "hot" to directly compare to the galaxy distribution. It is therefore not too useful to compare the mean infall velocity to the RMS velocity at a given distance. Rather we shall concentrate below on the low-order harmonics of the large-scale flow fields around clusters since these components are least affected by the necessary artificiality in the models of placing all the mass in the points.

All models except the anisotropic models behave in a nearly self-similar fashion so the choice of output time is not important. The typical expansion factor chosen for cluster examination was 4, which allowed clusters with a substantial number of points (> 1000) to form. The clusters were selected to match the properties of the Virgo cluster, namely that the $\bar{\delta} = 2$ radius should occur at 2–$3r_0$, where r_0 is defined by the correl-

ation function, $\xi(r_0) = 1$. In this way, we can conveniently keep the comoving length of the simulation cube to be $L = 1$. A further selection criterion was that the cluster should be isolated from other large clusters, as Virgo appears to be. In this goal we were never entirely successful; neighboring smaller clusters usually appear within the $\bar{\delta} = 1$ radius. This probably makes the models even more realistic since Virgo itself has several close but smaller neighbors such as the Ursa Major clouds, the Leo clouds, the Virgo II clouds and the N5866, N5676 clouds, all of which are subunits to the Virgo Supercluster (de Vaucouleurs 1975).

The clusters were chosen by visual inspection of the entire mass distribution of each model. The centers of the clusters were found by iterating the center of mass inside successively smaller spheres centered on the cluster. The particles in the simulations were then ordered by increasing distance from the cluster center and the mean interior overdensities $\bar{\delta}$ were computed.

$$1 + \bar{\delta}(r) = \frac{M(r)}{(4\pi/3)\rho_b r^3}, \tag{2}$$

where $M(r)$ is the mass inside a sphere of radius r centered on the cluster, and ρ_b is the background density of the universe. We bin the particles in shells of increasing overdensity. The shells are spaced evenly in log $\bar{\delta}$ so that the outermost shell is at $\bar{\delta} = 1$. For the innermost shell we include all particles inside the overdensity $\bar{\delta} \approx 12$. We use either eight or 16 shells depending on the richness of the clusters.

III. ANALYSIS

a) Pictures

Figures 1*a*–1*d* shows snapshots of the simulations at the output times used for the cluster analysis. Figures 1*a* and 1*b* show orthogonal projections of an $n = -2$ model after an expansion of 2.5, and Figures 1*c* and 1*d* are of the $n = -1$ model after an expansion factor of 4.0. The correlation length r_0 is 0.09 for the $n = -2$ model and 0.04 for the $n = -1$ model, whereas the correlation slopes are approximately $\gamma = 1.8$ for the $n = -2$ model, and $\gamma = 2.1$ for the $n = -1$ model (Frenk *et al.* 1986). Note in both models that there is considerable power on large scales and that none of the large clusters is very isolated. This is typical of all the models. The $n = -2$ models have very pronounced filamentary structure on large scales. The $n = -1$ models are less connected in their large-scale structure, and the individual clusters are therefore more isolated (Frenk *et al.* 1986). The CDM models have structure intermediate between these two cases. In all cases the degree of subclustering present is substantial on all scales. The $n = -2$ model appears more filamentary than observations, while the $n = -1$ model is perhaps less filamentary than the data. The range of velocity structure seen in these two models should therefore bracket that expected in the galaxy distribution.

We will look in detail at one large cluster from each of these models. Their centers are located at $(x_0, y_0, z_0) = (0.05, 0.26, 0.82)$ and $(0.29, 0.59, 0.49)$, respectively. Figures 2*a*–2*d* shows two projections of an area centered on each cluster with coordinates centered about each cluster, with the same projections as in Figure 1. For each particle we show the projection of the proper velocity

$$\boldsymbol{V}_{\text{proper}} = H a \boldsymbol{x} + a \frac{d\boldsymbol{x}}{dt},$$

where x are the comoving coordinates and a is the expansion factor. The scaling of the velocity vectors is arbitrary and was chosen for legibility. The eight circles are the overdensity contours defined by $\bar{\delta}_i = 2^{(i-1)/2}$.

Even the most cursory examination of Figure 2 shows that the velocity field is far from being purely radial and spherically symmetric. The velocity field of the first cluster is very strongly disturbed by the extensive subclustering. The two clusters in the lower right region of Figure 2*a* are tidally distorting the flow between their position and the central, more massive cluster, and a filament connecting the clusters is in the process of formation. Transverse velocities directed toward smaller subclusters are apparent as for example on the left sides of Figures 2*a* and 2*b*. From the vantage point of the cluster center, the flow pattern has dipole asymmetry directed toward the $(+x, -y)$ direction. Other higher order distortions are also apparent.

The cluster drawn from the $n = -1$ model is considerably more isolated, but even here the flow pattern is substantially distorted. Again from the vantage of the cluster center, there appears to be a dipole pattern directed toward the $(+x, +z)$ direction. Furthermore there are numerous subclumps within the $\bar{\delta} = 2$ surface which locally distort the flow pattern. The deviations from a spherical infall will be further elaborated below.

b) Spherically Averaged Infall

In spite of the substantial asphericity in the flow fields, one could still hope that the spherical model is applicable after averaging over the surface of the sphere. In Figures 3*a*–3*c* the solid curves plot the infall velocity expected in the spherical model as a function of overdensity $\bar{\delta}$ and Ω. The filled squares in each plot give the mean (averaged over solid angle; see below) dimensionless radial peculiar velocity $\bar{V}_r/Hr$ averaged over the nine anisotropic, the five isotropic CDM clusters, and the five clusters taken from the PPPM runs, respectively. We can average the clusters because the dimensionless infall velocity in spherical theory depends only on Ω and $\bar{\delta}$. The error bars give the standard deviation between the various clusters. The plots are essentially unchanged if we instead plot the mass-averaged infall of all particles on a shell.

The mean infall velocity for $\bar{\delta} \lesssim 2$ is characteristic for flow expected in spherical models with $\Omega = 0.9 \pm 0.1$, while for $2 \lesssim \bar{\delta} \lesssim 3$ the measured density would be $\Omega = 0.8 \pm 0.15$. These results are consistent with those found by Bushouse *et al.* (1985) and Lee, Hoffman, and Ftaclas (1986). As $\bar{\delta}$ increases the discrepancy becomes more pronounced. We thus see that $\bar{V}_r/Hr$ measures Ω quite well for small δ despite the fact that these models are not spherically symmetric. Conversely, however, in no cluster can we expect to apply the spherical model to regions with $\bar{\delta} > 4$. The spherical model is therefore reasonable for $\bar{V}_r/Hr < 1$ where the collapse has not yet turned around but rapidly becomes poor at smaller radii.

The isotropic and anisotropic CDM models (Figs. 3*a* and 3*b*) are essentially identical in their deviation from the spherical model, but the models evolved with the PPPM code show slightly more deviation from the spherical model expectations for all values of $\bar{\delta}$. The scatter between clusters is large, however, so this deviation may not be significant, but it might be expected because the PPPM models have stronger short-range forces so that the developing cluster can more readily transfer power from large- to small-scale degrees of freedom and become "previrialized" before it would have fully col-

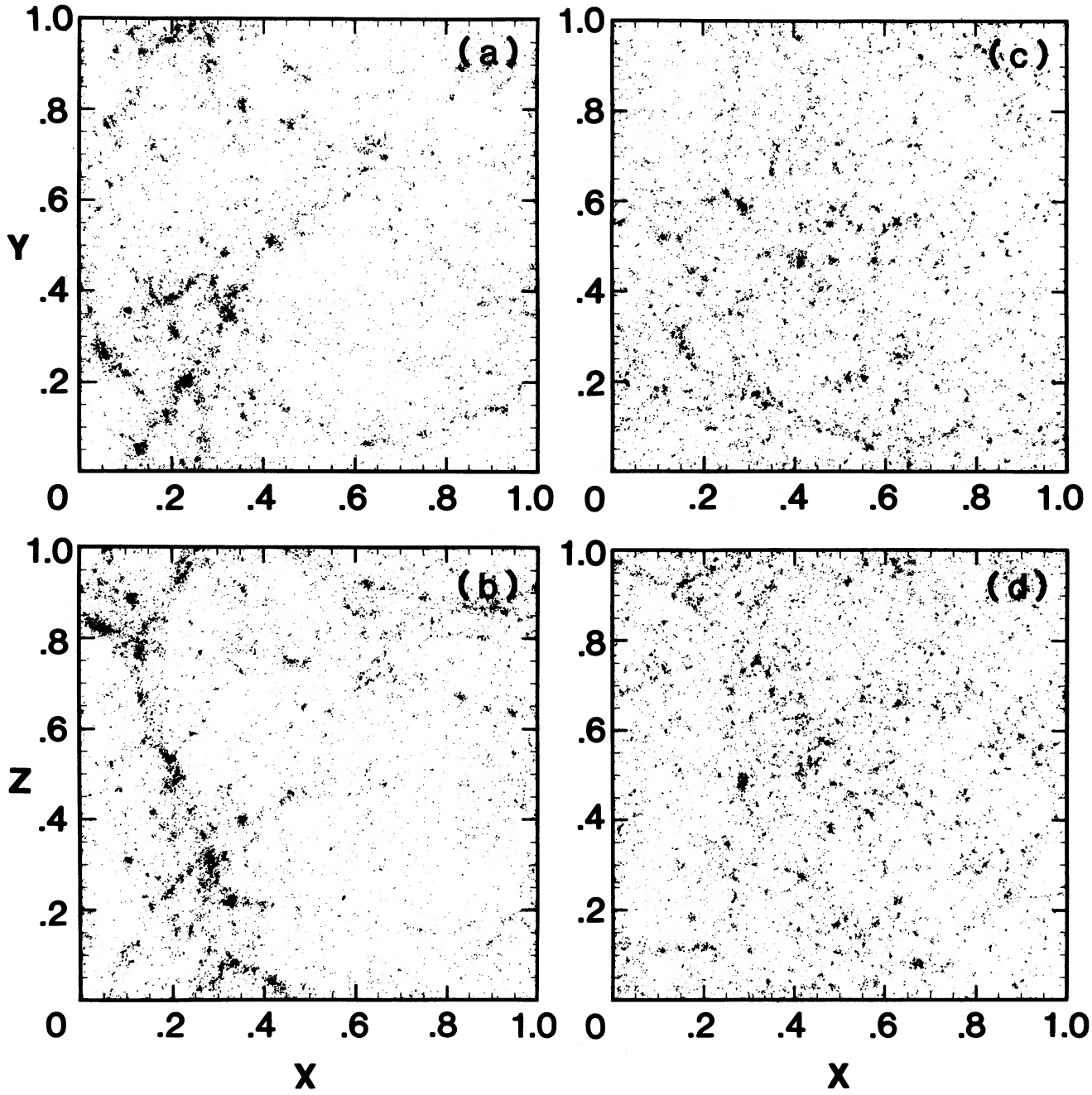

FIG. 1.—Cartesian projections of the PPPM simulations. Panels (*a*) and (*b*) are of the $n = -2$ model; (*c*) and (*d*) are of the $n = -1$ model. Panels (*a*) and (*c*) show X-Y projections, and (*b*) and (*d*) show X-Z projections.

lapsed according to spherical theory. $\bar{V}_r$ measures the mean-ordered "kinetic energy" of infall, but much of a particle's kinetic energy may be in the form of random "thermal energy" well before the cluster fully collapses.

c) *Deviations from Spherical Infall*

To illustrate the nature of the deviations from spherical infall, we plot in Figures 4*a*–4*d* the same clusters shown in Figure 2. Now, however, the vectors plotted for each point are the projected velocities after subtracting out the predictions of the spherical model. For this prediction we use the exact formula, not the analytic approximation, equation (1). All velocities are now relative to the mean of these points interior to the $\bar{\delta} = 11.3$ surface. The scaling of the length of the velocity vectors is identical to that used in Figure 2. The points interior to the $\bar{\delta} = 11.3$ surface are denoted as heavy solid points. The small-scale virialized motion around each subcluster is obviously pronounced as expected, but there is also considerable residual coherence in the large-scale motion.

It would be hopeless to try to give a full description of the deviations from spherical flow in each cluster, since that would depend upon the random position and mass of all the subunits. However, it is useful to characterize the gross deviations in terms of a few dimensionless numbers. To quantify the depar-

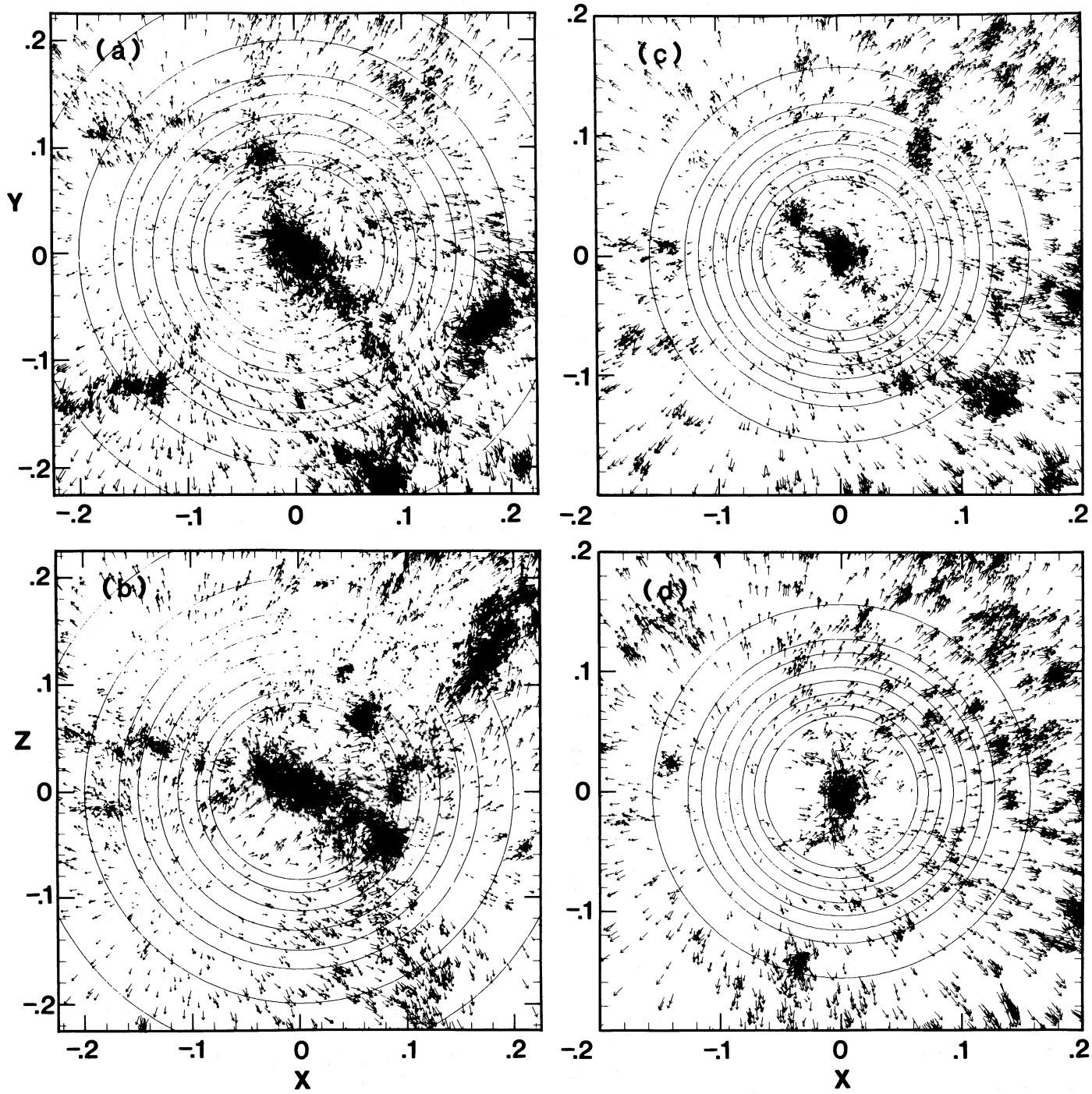

FIG. 2.—Cartesian projections of particles and velocities around clusters selected from Fig. 1. See text for positions of cluster centers. The vectors are proportional to the physical velocity of each point as seen from a comoving observer positioned at the cluster center. The axes have the same units as in Fig. 1. The eight circles are the overdensity contours defined by $\bar{\delta}_i = 2^{(i-1)/2}$.

tures from spherical symmetry, we expand the velocity and force fields around the clusters in terms of spherical harmonics on each shell. If the expansion is truncated beyond the quadrupole level, the fluctuations are effectively smoothed on scales less than 90° so that most details for each cluster are filtered out, while the large-scale structure of the flow field is preserved. Since these are vector fields we can separately consider the radial and transverse components V_r and V_t, F_r and F_t. For the most part we are interested in the radial components, so we need consider only the spherical harmonics of a scalar field,

$$V_r(\theta, \phi) = \sum_{n=0}^{\infty} \sum_{m=-n}^{n} V_r^{n,m} P_n^m(\cos\theta) \exp(im\phi) , \quad (3)$$

$$V_r^{n,m} = \left[\frac{2n+1}{4\pi} \frac{(n-|m|)!}{(n+|m|)!}\right] \int_0^{\pi} \int_0^{2\pi} V_r(\theta, \phi) P_n^m(\cos\theta) \times \exp(-im\phi) \sin\theta d\phi d\theta , \quad (4)$$

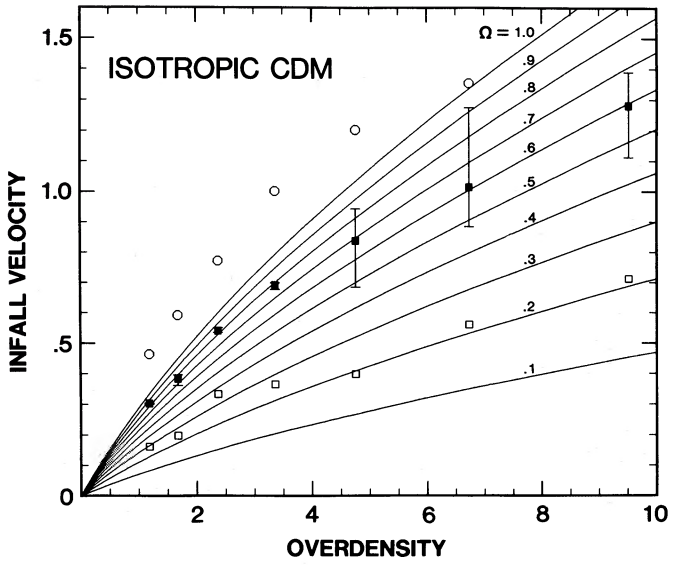

FIG. 3*a*

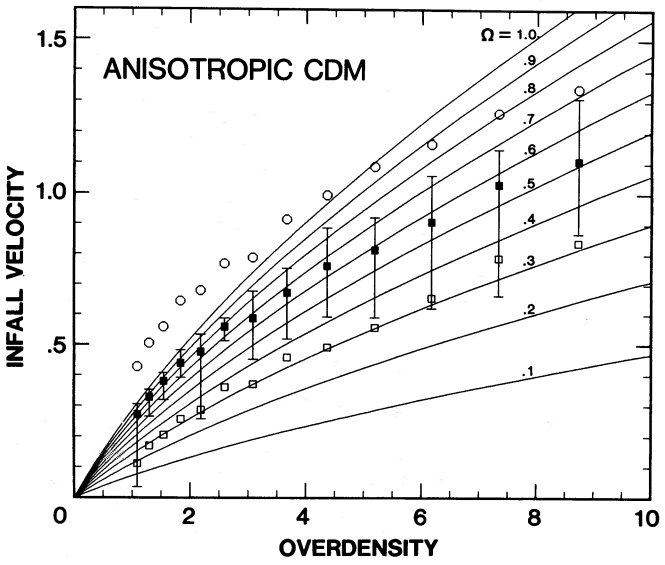

FIG. 3*b*

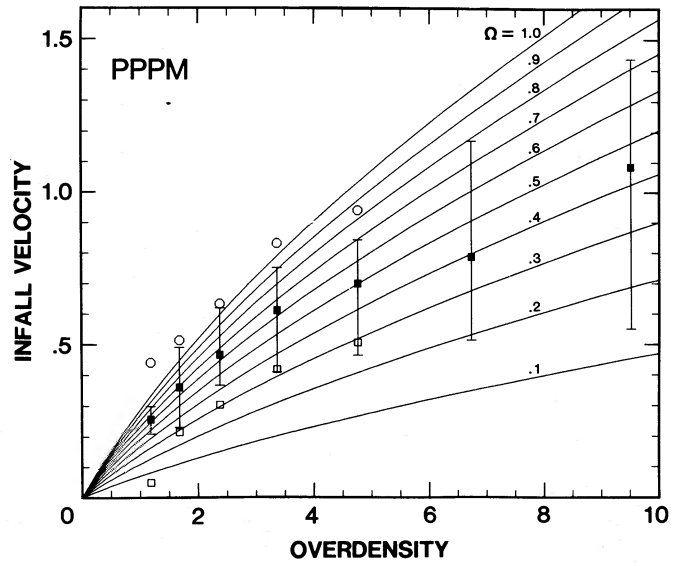

FIG. 3*c*

FIG. 3.—(*a*) The measured mean radial infall $\bar{V}_r/Hr$ for the isotropic CDM models evolved with the PM code. The error bars denote the scatter between clusters. The open symbols show the infall as would be measured along the major or minor axes of the best-fitting quadrupole distortion at each overdensity. The expectations of exact spherical symmetry are shown as the smooth curves for various values of Ω. (*b*) The same as Fig. 3*a*, now for the anisotropic CDM models evolved with the PM code. (*c*) The same as Fig. 3*a*, now for the power-law initial conditions evolved with the PPPM code.

where P_n^m are associated Legendre polynomials. We will define the infall velocity as minus the radial velocity to avoid confusion.

The force field is defined on a grid in the n-body codes, and it is easy to interpolate between grid points to compute the force at any point. However, a complication arises in the orthogonality of the velocity terms because of the nonuniform distribution of particles. If the velocity coefficients in equations (3)–(4) are determined by direct summation over all particles, nonzero quadrupole terms could result even in the case of spherically symmetric infall should the density not be constant over the sphere. To avoid this problem we divide the sphere into 128 equal areas that are equally spaced in cos θ and in ϕ. The contribution to the velocity terms in each area is then normalized by the number of particles in that area. In this way the effect of tangential density gradients is greatly reduced.

In a mirror symmetric collapse we expect V_r to also show mirror symmetry. In a collapse with mirror symmetry around the x-y plane we expect the tangential velocity V_t to be zero at the z-axis and in the x-y plane. Furthermore we expect V_t to be antisymmetric around $\theta = \pi/2$. This indicates that the monopole term is zero and that the simplest axisymmetric approximation to V_t using spherical harmonics is

$$V_t(\theta) = V_t^{2,0}[P_1(\cos\theta) - P_3(\cos\theta)]$$
$$= V_t^{2,0} 2.5(\cos\theta - \cos^3\theta) = V_t^{2,0}\,\tfrac{5}{4}\sin\theta\sin 2\theta\,. \quad (5)$$

This component of V_t and F_t was computed for each shell, choosing the z-axis as the minor axis of the radial velocity or force. Because the flow is compressible there is no simple relation between $V_t^{2,0}$ and $V_r^{2,0}$.

These distortions are irrotational, and it is also of interest to measure the circulation of the flow. For this we compute

$$V_c = \frac{1}{N}\sum_i \frac{V_i \times r_i}{r_i}\,, \quad (6)$$

where the sum extends over the N particles in a given shell.

Listed in Table 1 are the rms amplitudes of the dipole ΔV_r^1, $[(\Delta V_r^1)^2 = \sum_m (\Delta V_r^{1,m})^2]$, radial quadrupole ΔV_r^2 and $V_t^{2,0}$, and circulation $|V_c|$ when averaged over all clusters for various values of $\bar{\delta}$. The anisotropic CDM, isotropic CDM, and PPPM clusters are tabulated separately, and the errors are the standard deviations when averaged across the clusters. Each of these velocities has been made dimensionless by dividing by the predicted spherical infall $\bar{V}_r$ at a given radius. The ΔV_r for the dipole and quadrupole terms is the difference between the maximum and minimum infall velocities on the sphere for the harmonic in question. Note that these dimensionless distortions are not particularly small. The dipole distortions are seen to increase with $\bar{\delta}$ in all models, although the scatter increases substantially with $\bar{\delta}$. The other terms are nearly independent of

TABLE 1

ANISOTROPY AMPLITUDE

Model	$\Delta V_r^1/\bar{V}_r$	$\Delta V_r^2/\bar{V}_r$	$V_t^{2,0}/\bar{V}_r$	$\lvert V_c\rvert/\bar{V}_r$
Isotropic:				
$\bar{\delta}=2$.....	0.36 ± 0.01	0.81 ± 0.21	0.11 ± 0.08	0.10 ± 0.01
$\bar{\delta}=4$.....	0.50 ± 0.15	0.90 ± 0.42	0.16 ± 0.13	0.11 ± 0.08
$\bar{\delta}=8$.....	0.80 ± 0.29	0.80 ± 0.14	0.17 ± 0.11	0.13 ± 0.07
Anisotropic:				
$\bar{\delta}=2$.....	0.38 ± 0.17	0.80 ± 0.22	0.36 ± 0.16	0.10 ± 0.07
$\bar{\delta}=4$.....	0.28 ± 0.08	0.66 ± 0.23	0.31 ± 0.12	0.21 ± 0.11
$\bar{\delta}=8$.....	0.64 ± 0.40	0.43 ± 0.14	0.35 ± 0.20	0.22 ± 0.09
PPPM:				
$\bar{\delta}=2$.....	0.32 ± 0.10	0.50 ± 0.48	0.25 ± 0.18	0.09 ± 0.04
$\bar{\delta}=4$.....	0.74 ± 0.34	0.45 ± 0.36	0.18 ± 0.14	0.21 ± 0.09
$\bar{\delta}=8$.....	0.87 ± 0.44	0.32 ± 0.28	0.25 ± 0.32	0.33 ± 0.08

$\bar{\delta}$. The most important point to note is that the dimensionless distortions seem relatively independent of the class of n-body model. An exception to this could be the radial quadrupole distortion, although the scatter across the clusters is large.

To calibrate the distortions, consider the circulation, which is typically a 10%–20% effect at the $\bar{\delta}=2$ surface. Scaled to the Virgo Cluster, this would be a transverse circulation velocity of 75–150 km s^{-1} for galaxies at our Virgocentric radius and overdensity surface. The typical irrotational transverse velocity would be of the same order, the typical dipole term would contribute effects of order ± 130 km s^{-1}, and the radial quadrupole distortion would be nearly twice as large. These effects are by no means negligible and could explain the bulk of our transverse velocity within the local supercluster.

An illustration of the effect of the radial quadrupole distortions is shown in Figure 3. The solid points in Figures 3*a*–3*c* show the mean infall when averaged over 4π sr for each overdensity. The open octagons and squares on Figures 3*a*–3*c* denote the infall as seen along the major and minor axes of the radial quadrupole distortion which best fits each cluster. The scatter about the mean is not plotted but is similar to that for the spherical infall curves. The point to note is that the radial quadrupole distortions of typically $\pm 40\%$ (Table 1) are very substantial deviations to the mean flow that can lead to infall estimates wrong by a factor of 2 if points are not sampled over 4π sr.

We attempted to correlate the deviations from spherical flow with a number of other observable parameters, mostly with poor results. For example, the quadrupole distortion of the velocity field did not always align well with the quadrupole distortion of the force field, particularly in the isotropic models for which the distortions were only occasionally well described by a quadrupole field. Originally we had thought there would be reasonable alignment of the quadrupole distortions with the moment of inertia tensor of the interior mass distribution, but in fact there was virtually no correlation at all, for a variety of radial weightings of the inertia tensor. The poor correlation is undoubtedly due to the significant contribution to the force field from the exterior matter.

IV. FORCE AND VELOCITY ALIGNMENT

After we realized that the departures from spherical symmetry were not adequately described by distortions to quadrupole order, we despaired until we realized we should consider a much simpler statistic. In linear theory the expected peculiar velocity $\boldsymbol{v}_p$ of a particle will be parallel to the peculiar force vector $\boldsymbol{F}$ and is given by (Peebles 1980)

$$\boldsymbol{v}_p = \frac{2}{3\Omega^{0.4}H_0}\boldsymbol{F} \tag{7}$$

We can test the validity of linear theory by calculating the ratio α

$$\alpha = \left(\frac{2}{3\Omega^{0.4}H_0}\right)\frac{\boldsymbol{v}_p \cdot \boldsymbol{F}}{|\boldsymbol{F}^2|} \tag{8}$$

for observed velocities and forces. In linear theory this ratio is unity. We are also interested in the degree of parallelism between the force and velocity vectors so we computed the mean value of the cosine of the angle between the force and velocity vectors. In order to test how well the deviations from the simple spherical model obey linear theory we subtract the simple spherical model from the force field and the velocity field. We subtract the monopole term $(4\pi/3)G\bar{\delta}\rho_b \boldsymbol{r}$ from the force field. The expected radial velocity in the exact spherical model is subtracted from the observed velocity field. We divide each overdensity shell into 64 segments of equal area to derive volume averaged values. In order to diminish the effects of local nonlinearities induced by subclustering we consider only segments with less than 10 particles in them. If all segments were included, the alignment would be reduced because there need be no alignment between force and velocity within virialized subsystems. Figures 5*a*, 5*c*, and 5*e* show the mean value of cosine of the angle between the force and velocity vectors as a function of overdensity. Results for the anisotropic CDM, isotropic CDM, and PPPM clusters are again plotted separately. The error bar is the scatter between the clusters. The solid triangles show that the vectors are very well aligned. Up to an overdensity of $\bar{\delta}=4$ the alignment is typically better than 25° with relatively little scatter. With the open triangles the simple spherical model is subtracted. We see that the alignment is not quite as good, and the scatter is increased, but it is still excellent.

Figures 5*b*, 5*d*, and 5*f* show the ratio α defined in equation (8) averaged over the clusters for each class of model. Note that $\alpha < 1$ in the nonlinear regime and that there is an excellent correlation between this ratio and the mean interior overdensity for the various models. The scatter between clusters is again relatively small, 0.05. When the simple nonlinear spherical model is subtracted, the scatter is considerably larger between the various models, but we see the same overall trend with overdensity. The smooth curve indicates the ratio we would observe for the simple nonlinear spherical model. This curve tracks the data remarkably well, in spite of the fact that the fluctuations, particularly the open symbols, can be highly nonspherical. This behavior is consistent with the expectations of second-order perturbation analysis (Tomita 1967). The three classes of models are seen to behave in a completely consistent fashion. The scatter is larger in the PPPM models than in the PM models, again probably because of increased small-scale structure.

That equations (7)–(8) are a good description of the aspherical flow velocity should, on hindsight, be no surprise, as it is equivalent to the Zel'dovich (1970) approximation, which is known to exactly describe one-dimensional pancake collapse up to the point of caustic formation. Efstathiou and Silk (1983) demonstrated that the Zel'dovich approximation alone gives an excellent description of large-scale kinematics in three-

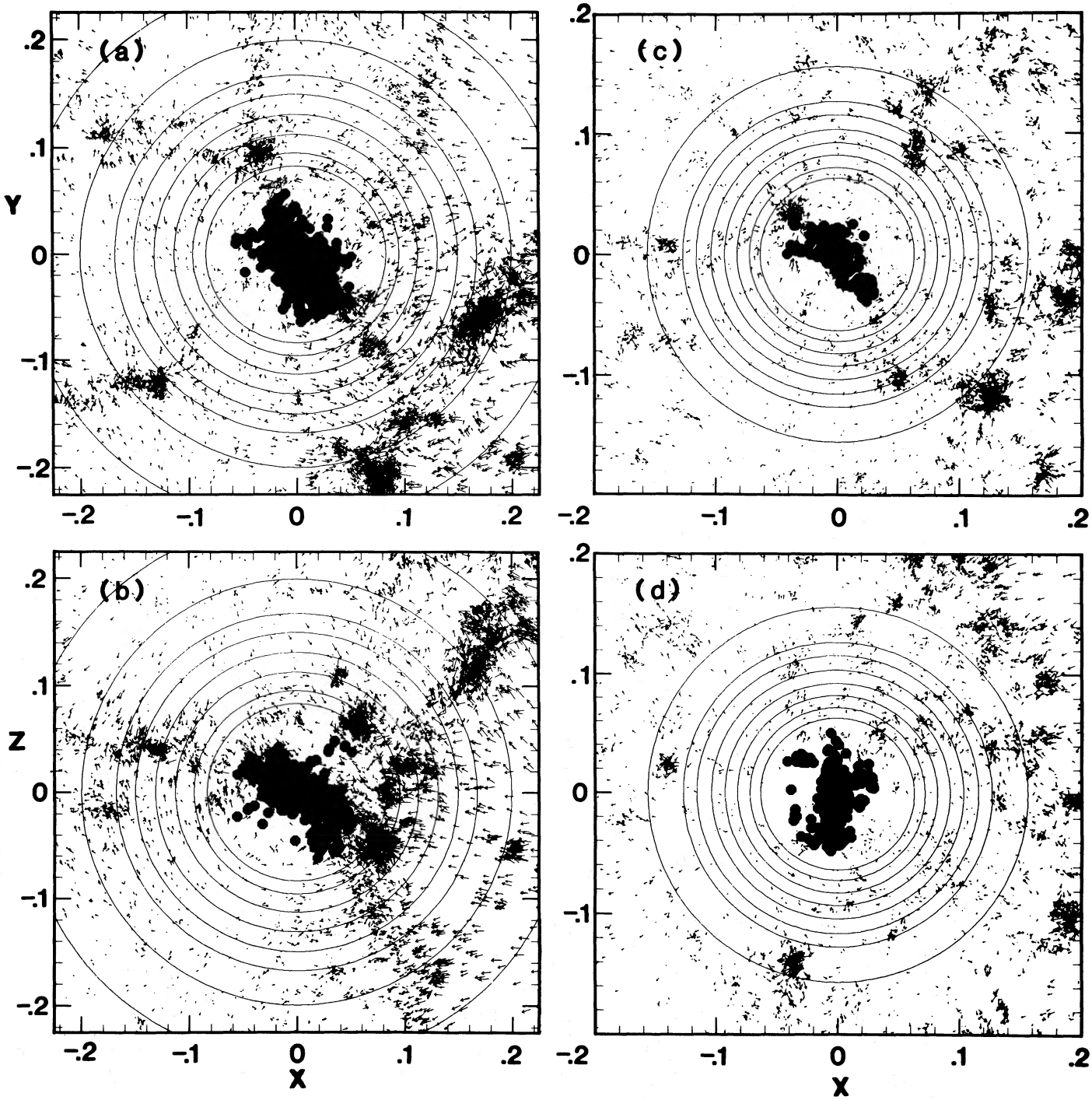

FIG. 4.—The same cluster as shown in Fig. 2, now with the spherical model infall component removed and with the velocities relative to the mean of the points within the $\bar{\delta} > 11.3$ surface.

dimensional models, but of course it cannot be expected to apply to highly nonlinear, collapsed regions.

V. APPLICATION TO THE VIRGO SUPERCLUSTER FLOWFIELD

Whether the large-scale distortions lead to an increase or decrease of the mean infall of galaxies near the observer depends less on the interior mass distribution than on the exterior distribution. The fact that the local group of galaxies lies on the flattened supercluster plane does not necessarily mean that our infall should be increased by the flattened galaxy (and mass?) distribution interior to us. In the absence of an exterior field, potential theory would suggest our infall velocity to be higher than average for the sphere, but if the supercluster plane extends to larger radii, our infall should be smaller than the average over the sphere (Peebles 1980). The aspherical distortions do not necessarily bias the mass estimation of the cluster in a given direction, but they definitely increase the statistical uncertainty of the estimates based on

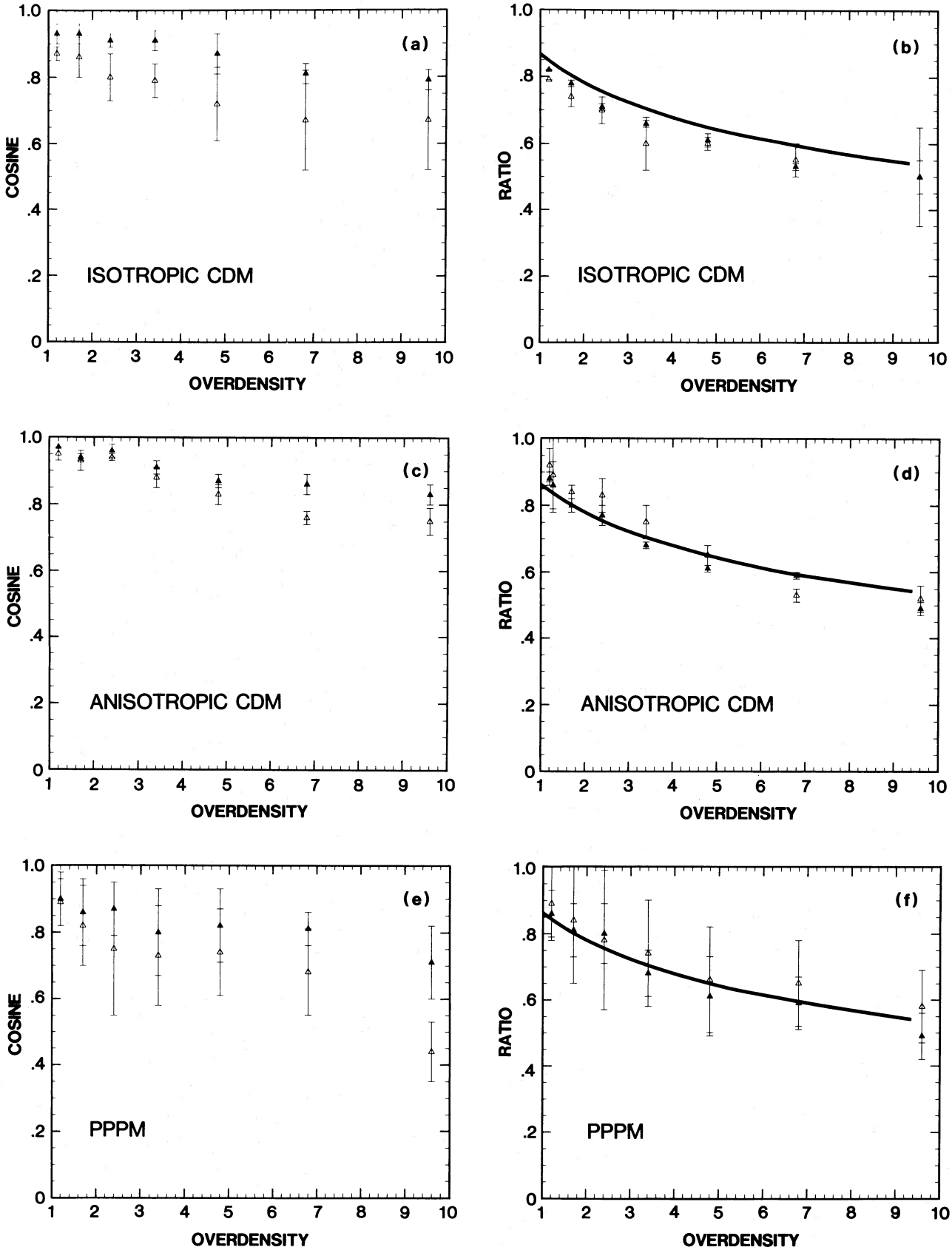

FIG. 5.—The relation of the average local force and velocity as a function of $\bar{\delta}$. Figs. 5*a*, 5*c*, and 5*e* plot the average of the cosine between local force and velocity vectors; Figs. 5*b*, 5*d*, and 5*f* plot the average of the ratio of peculiar velocity to peculiar force. The smooth curve is the expected ratio for the spherical, nonlinear model. The error bars show the scatter across clusters. The open symbols and errors are the averages after subtracting out the spherical infall. Figs. 5*a* and 5*b* plot the isotropic CDM models, Figs. 5*c* and 5*d* plot the anisotropic CDM models, and Figs. 5*e* and 5*f* plot the PPPM models.

spherical infall theory. A $\pm 50\%$ variation in the local infall value, which is the typical fluctuation of the n-body clusters, leads to an error of mass or Ω estimation by a factor of 3. An error this large would obviate the possibility of using this test to set any useful constraint on Ω.

The asphericities in the flow field would be less of a problem if we could sample galaxies with equal weight from 4π sr around Virgo. In practice, however, this is rather difficult to arrange. Not only are the galaxies preferentially distributed on the supercluster plane, but the galaxies near to us on the front side of the cluster have far more weight than those on the back side of the cluster. Furthermore, the back side galaxies are usually deleted from the fits because they are in the triple value zone (Schechter 1980; Yahil, Sandage, and Tammann 1980; Tonry and Davis 1981; Aaronson *et al.* 1982). The net result is that the harmonic distortions (e.g. dipole) are not orthogonal to the monopole infall and the monopole fit must have a random uncertainty at least as large as the amplitude of the dipole distortion.

There is one systematic bias that is definitely present in the fits to the spherical flow models. As seen in Figure 3, the mean infall of the n-body clusters is somewhat below the spherical model, and the fractional deviation increases with $\bar{\delta}$. Only the spatial gradient of the peculiar flow field is observable; solid body rotation, for example, would not be detectable through measurement of anisotropy of the Hubble flow. A good deal of weight to the measured infall comes from galaxies within our Virgocentric radius. Our results demonstrate that the spherically averaged infall of these galaxies is expected to be lower than predicted by the spherical model; fitting the incorrect model leads directly to a systematic underestimate of our own infall velocity and Ω: The seriousness of the bias depends upon the proximity of these inner galaxies to Virgo. A remedy would be either to use the infall curve found for our models in the fits, or to delete those galaxies within the $\bar{\delta} \approx 3$ surface. Deleting the inner galaxies would likely result in substantially larger statistical error for our derived infall. The details of these considerations may be somewhat modified in $\Omega < 1$ models, which remains the subject of another paper.

The only encouraging result from this study is that there is a simple replacement of the spherical model that readily deals with the asphericity of the flow field, namely the excellent correlation of peculiar velocity with peculiar gravity. To apply this method will require a full sky sample of galaxies with redshifts, from which the peculiar gravity can be directly computed on a shell by shell basis (assuming of course that the galaxies of the sample roughly trace the mass). It is probably preferable to give each galaxy equal weight after at least partially volume limiting the sample. Davis and Huchra (1982) used this technique to compute the component of peculiar acceleration directed toward the galactic pole using the CfA redshift survey galaxies in the north, and the shallower Shapley-Ames catalog in the south. They found the peculiar gravity converged just on the back side of the Virgo cluster, which totally dominated this component of acceleration, even though the shells extended to $80h^{-1}$ Mpc.

A much better sample for his analysis are the galaxies detected by the *IRAS* satellite at 60 μm. Recently it has been shown (Yahil, Walker, and Rowan-Robinson 1985; Meiksin and Davis 1986) that there is a robust dipole anisotropy in the angular distribution of these galaxies that points within 30° of the microwave dipole anisotropy and 37° from the center of Virgo. The *IRAS* sample is deep enough to measure our total expected peculiar acceleration, which should be compared to our total peculiar velocity, as inferred from the microwave dipole anisotropy.

If the *IRAS* galaxies do roughly trace the mass distribution then our peculiar gravity should be directed close to the *IRAS* anisotropy, and the 30° misalignment with our peculiar velocity is precisely the typical deviation seen in the n-body models. The anisotropy of the *IRAS* catalog appears to be dominated by fluctuations within $50h^{-1}$ Mpc of us and possibly even by material within $30h^{-1}$ Mpc loosely associated with the Virgo Supercluster. A very powerful cosmological test will be to measure the redshifts of the *IRAS* galaxies in order to accurately compute our peculiar acceleration. The usual caveat applies that one assumes the *IRAS* galaxies to trace the large-scale matter distribution. If the matter is less clustered than the sample, the Ω derived will be an underestimate of the total Ω, and vice-versa.

The prospects for an independent measure of our peculiar velocity derived from Hubble anisotropy appear less promising. Unless second distance indicators can be made much better than any available today, it will always be necessary to fit to a detailed model of the flowfield, but no simple flowfield is likely to be a reliable model of the Local Supercluster. One alternative is to fit simply for a dipole pattern that is the reflection of our peculiar velocity relative to a distant set of clusters spaced around the sky. Aaronson *et al.* (1986) have used the IR Tully-Fisher technique for 10 clusters at distances ranging from $40h^{-1}$ to $100h^{-1}$ Mpc, and they find a dipole velocity of 800 ± 200 km s^{-1} in a direction close to the microwave result. Although the significance of this result is low the agreement is encouraging and suggests that the microwave dipole anisotropy is entirely generated by inhomogeneities within the radius of these clusters, as expected from the *IRAS* catalog (Meiksin and Davis 1986). It may prove extremely difficult to improve upon the Aaronson *et al.* result.

VI. SUMMARY

We have studied the velocity fields around rich clusters in n-body simulations and have reached the following conclusions:

1. The clusters forming from random phase initial conditions are always subclustered and are never isolated. They are usually triaxial.

2. The flowfields when averaged over 4π sr fit spherical infall models relatively well for $\bar{\delta} < 3$, but the mean infall is systematically low for increasing $\bar{\delta}$.

3. The flowfields have substantial asphericity on large and small scale. An expansion of the aspherical velocity field in terms of spherical harmonics up to the quadrupole order yields amplitudes of the radial and transverse distortions in the range of 20%–50% of the mean infall velocity.

4. The asphericities in the flowfield are poorly correlated with the inertial tensor of the interior mass distribution, indicating they are largely influenced by the exterior mass distribution.

5. In spite of the serious local diviations from the spherical models which occur on all shells of overdensity $\bar{\delta}$, the local peculiar velocity field is extremely well aligned with the local force field, as would be expected in linear perturbation theory. For those points with $\bar{\delta} < 4$, not embedded in dense subclusters, the mean deviation of force and velocity vectors is only 25°; the ratio of the amplitudes is close to that expected by equation (1).

The n-body models from which these results were derived do produce large-scale structure that is a reasonable match to observations, and the large clusters contained within them are perhaps a reasonable match to large clusters such as Virgo. If this is so, then our results have several implications for study of Virgocentric flow:

1. Unless galaxies are drawn from 4π sr around Virgo the spherical model is unlikely to describe accurately the mean infall for any $\bar{\delta}$. Since this is impossible to achieve in practice there is to be expected a 50% random error of the mean infall for any $\bar{\delta}$ surface, which translates to a mass uncertainty of a factor 3.

2. The fact that the mean infall for $\bar{\delta} > 3$ is somewhat lower than predicted by the spherical model leads to a smaller observable shear field in the Hubble flow and systematic underestimation of the cluster mass when fitting a simple spherical infall model to the observations.

3. The most reliable measure of mass in the Virgo Supercluster is likely to result from a comparison of our peculiar force with our total peculiar velocity, namely the microwave dipole anisotropy. Perhaps the galaxy catalog derived from the *IRAS* data base (Yahil, Walker, and Rowan-Robinson 1986; Meiksin and Davis 1986; Davis 1986), which is drawn from much larger solid angle than is possible from optically selected catalogs, will eventually yield an accurate estimate of the peculiar gravitational force acting on our local group of galaxies.

We acknowledge helpful suggestions from J. Silk. M. D. thanks his n-body collaborators S. White, G. Efstathiou, and C Frenk for allowing him to play with some unpublished models. We thank Avery Meiksin, Rosie Wyse, Nicola Vittorio, and Ed Bertschinger for comments on the text. This research was supported in part by NSF grants AST-8419910, PHY-8440263, and by DOE contract DE-FG03-84ER40161.

REFERENCES

Aaronson, M., Bothun, G., Mould, J., Huchra, J., Schommer, R. A., and Cornell, M. E. 1986, *Ap. J.*, **302**, 536.
Aaronson, M., Huchra, J., Mould, J., Schechter, P., and Tully, B. 1982, *Ap. J.*, **258**, 64.
Bardeen, J. M., Bond, J. R., Kaiser, N., and Szalay, A. S. 1986, *Ap. J.*, **304**, 15.
Blumenthal, G. P., and Primack, J. P. 1983, in *Fourth Workshop on Grand Unification*, ed. H. D. Weldon, P. Langacker, and P. J. Steinhardt (Boston: Birkhausen), p. 256.
Bushouse, H., Melott, A. L., Centrella, J., and Gallagher, J. S. 1985, *M.N.R.A.S.*, **217**, 7P.
Davis, M. 1986, in *Dark Matter in the Universe, IAU Symposium 117*, ed. J. Knapp and J. Kormendy (Dordrecht: Reidel), in press.
Davis, M., Efstathiou, G., Frenk, C., and White, S. 1985, *Ap. J.*, **292**, 371.
Davis, M., and Huchra, J. 1982, *Ap. J.*, **254**, 425.
Davis, M., Lecar, M., Pryor, C., and Witten, E. 1981, *Ap. J.*, **250**, 423.
Davis, M., and Peebles, P. J. E. 1983, *Ann. Rev. Astr. Ap.*, **21**, 109.
de Vaucouleurs, G. 1975, in *Stars and Stellar Systems*, Vol. **9**, *Galaxies and the Universe*, ed. A. Sandage, M. Sandage, and J. Kristian (Chicago: University of Chicago Press), p. 557.
de Vaucouleurs, G., and Peters, W. L. 1984, *Ap. J.*, **287**, 1.
Dressler, A. 1984, *Ap. J.*, **281**, 512.
Efstathiou, G. 1985, *M.N.R.A.S.*, **213**, 29P.
Efstathiou, G., Davis, M., Frenk, C. S., and White, S. D. M. 1985, *Ap. J. Suppl.*, **57**, 241.
Efstathiou, G., and Silk, J. 1983, *Fund. Cosmic Phys.*, **9**, **1**.
Fixsen, D. J., Cheng, E. S., and Wilkinson, D. T. 1983, *Phys. Rev. Letters*, **50**, 620.
Frenk, C. S., Efstathiou, G., White, S. D. M., and Davis, M. 1986, in preparation.
Gelmini, G., Schramm, D. N., and Valle, J. W. F. 1984, *Phys. Letters*, **146B**, 311.
Kaiser, N. 1984, *Ap. J. (Letters)*, **284**, L9.
Lee, H., Hoffman, Y., and Ftaclas, C. 1986, *Ap. J. (Letters)*, **304**, L11.
Lubin, P. M., Epstein, G. L., and Smoot, G. F. 1983, *Phys. Rev. Letters*, **50**, 616.
Meiksin, A. 1985, private communication.
Meiksin, A., and Davis, M. 1986, *A.J.*, **91**, 191.
Melott, A. 1983, *M.N.R.A.S.*, **205**, 637.
Olive, K. A., Seckel, D., and Vishniac, E. 1985, *Ap. J.*, **292**, 1.
Peacock, J. A., and Heavens, A. F. 1985, preprint.
Peebles, P. J. E. 1980, *The Large Scale Structure of the Universe* (Princeton: Princeton University Press).
Schechter, P. 1980, *A.J.*, **85**, 801.
Silk, J. 1974, *Ap. J.*, **193**, 525.
———. 1977, *Astr. Ap.*, **59**, 53.
Suto, Y., Kodama, H., and Sato, K. 1985, *Phys. Letters*, **157B**, 259.
Szalay, A., and Silk, J. 1983, *Ap. J. (Letters)*, **264**, L31.
Tammann, G. A., and Sandage, A. 1985, *Ap. J.*, **294**, 81.
Tomita, K. 1967, *Prog. Theoret. Phys.*, **37**, 831.
Tonry, J., and Davis, M. 1981, *Ap. J.*, **246**, 680.
Turner, M. S., Steigman, G., and Krauss, L. M. 1984, *Phys. Rev. Letters*, **52**, 2090.
Villumsen, J., and Gunn, J. 1985 in preparation.
Vittorio, N., and Silk, J. 1985, *Ap. J. (Letters)*, **293**, L1.
White, S. D. M., and Silk, J. 1979, *Ap. J.*, **231**, 1.
Yahil, A. 1985, in *The Virgo Cluster of Galaxies*, ed. O. G. Richter and B. Binggeli, (Garching: European Southern Observatory), p. 359.
Yahil, A., Sandage, A., and Tammann, G. 1980, *Ap. J.*, **242**, 448.
Yahil, A., Walker, D., and Rowan-Robinson, M. 1986, *Ap. J. (Letters)*, **301**, L4.
Zel'dovich, Y. B. 1970, *Astr. Ap.*, **5**, 84.

MARC DAVIS: Department of Astronomy, Campbell Hall, University of California, Berkeley, CA 94720

JENS VILLUMSEN: Theoretical Astrophysics Group, 130-33 Cal Tech, Pasadena, CA 91125